Research Article

Nano Research
2021, 14(2): 512–517

ISSN 1998-0124 CN 11-5974/O4
https://doi.org/10.1007/s12274-020-2794-9

A robust soc-MOF platform exhibiting high gravimetric uptake and volumetric deliverable capacity for on-board methane storage

Gaurav Verma[1], Sanjay Kumar[1,†] (✉), Harsh Vardhan[1], Junyu Ren[1], Zheng Niu[1], Tony Pham[1,‡], Lukasz Wojtas[1], Sydney Butikofer[1,⊥], Jose C Echeverria Garcia[1], Yu-Sheng Chen[2], Brian Space[1], and Shengqian Ma[1] (✉)

[1] *Department of Chemistry, University of South Florida, 4202 E. Fowler Ave., Tampa, FL 33637, USA*
[2] *ChemMatCARS, Center for Advanced Radiation Sources, The University of Chicago, 9700 South Cass Avenue, Argonne, IL 60439, USA*
[†] *Present address: Department of Chemistry, Multani Mal Modi College, Patiala 147001, India*
[‡] *Present address: Department of Chemistry, Biochemistry, and Physics, The University of Tampa, 401 W. Kennedy Blvd., Tampa, FL 33606-1490, USA*
[⊥] *Present address: Department of Chemical and Biomolecular Engineering, University of Illinois at Urbana-Champaign, Champaign, IL 61801, USA*

Received: 1 February 2020 / **Revised:** 24 March 2020 / **Accepted:** 2 April 2020

ABSTRACT

Emerging as an outperformed class of metal-organic frameworks (MOFs), square-octahedron (**soc**) topology MOFs (soc-MOFs) feature superior properties of high porosity, large gas storage capacity, and excellent thermal/chemical stability. We report here an iron based soc-MOF, denoted as Fe-pbpta (H_4pbpta = 4,4′,4″,4‴-(1,4-phenylenbis(pyridine-4,2-6-triyl))-tetrabenzoic acid) possessing a very high Brunauer, Emmett and Teller (BET) surface area of 4,937 m^2/g and a large pore volume of 2.15 cm^3/g. The MOF demonstrates by far the highest gravimetric uptake of 369 cm^3(STP)/g under the DOE operational storage conditions (35 bar and 298 K) and a high volumetric deliverable capacity of 192 cc/cc at 298 K and 65 bar. Furthermore, Fe-pbpta exhibits high thermal and aqueous stability making it a promising candidate for on-board methane storage.

KEYWORDS

metal-organic framework (MOF), reticular chemistry, methane storage, aqueous stability, high gravimetric and volumetric uptake

1 Introduction

In the present scenario, the environmental concern and climate change are at defining moment due to the increase in the average global temperature leading to unprecedented weather pattern and rising sea level [1, 2]. The injudicious use of fossil fuels in the energy production and automobile sector has resulted in the sharp increase of atmospheric carbon dioxide (> 400 ppm) causing some environmental and health issues. Therefore, the immediate shift towards environmental benign green resources, like natural gas (consisting of mainly methane, ~ 95%), is the need of the hour [3]. Due to the natural abundance and low carbon dioxide emission, the use of natural gas in automobile industry has gained escalating interest. However, the low volumetric energy density of methane or natural gas deterred its utilization as fuel. The strategies i.e. the use of liquified natural gas (LNG) and compressed natural gas (CNG), to address this impediment are also associated with drawbacks like high cost for cryogenic processes, heavy and expensive vessels, and risks of explosion. Another approach of adsorption of natural gas (ANG) using porous materials has emerged as potential alternative to solve these problems [4, 5].

The last two decades have witnessed enormous advances in the field of porous materials, specifically the development of framework materials i.e. metal-organic frameworks (MOFs) and covalent organic frameworks (COFs) [6–9]. The introduction of reticular chemistry by Yaghi et al. [10, 11] is one of the most critical aspect of this acclamatory progress, leading to the discovery and development of highly functional crystalline materials, particularly MOFs [12]. MOFs are the class of materials generated by combination of metal nodes (metal ions or metal clusters known as secondary building units, SBUs) and bi/multidendate organic linkers [13, 14].

Due to their crystallinity, structural diversity, high porosity, ease of functionalization and presence of a high density of binding sites, MOFs become promising candidates for gas storage and separation [4, 12, 15–18]. Early examples include HKUST-1 [16, 19] that showed the highest volumetric uptake capacity of 267 cc/cc at 65 bar and room temperature. From there on, numerous MOFs with high volumetric uptake under these conditions have been reported such as PCN-14 [20] (230 cc/cc), UTSA-76a [21] (257 cc/cc), MAF-38 [22] (263 cc/cc) and Ni-MOF-74 [16] (251 cc/cc). The U.S. Department of Energy (DOE) set the storage target of 263 cm^3(STP)/cm^3 at 65 bar, which seems practical, and has been achieved, but the efficiency of the adsorbent material depends on their deliverable capacity (between 5 and 65 bar). Among the uncountable MOFs materials, a very few MOFs with high volumetric deliverable capacity have been reported till date such as MOF-519 [23] (209 cc/cc), NJU-Bai-43 [24] (198 cc/cc), Co(bdp) [25] (197 cc/cc) and UTSA-76a [21] (197 cc/cc) among many others [18, 24, 26, 27]. Furthermore, without high operational and thermal stability,

Address correspondence to Shengqian Ma, sqma@usf.edu; Sanjay Kumar, sanjay2002@gmail.com

the practical usage of frameworks seems farfetched.

In this context, iron-containing metal-organic frameworks (Fe-MOFs) with square-octahedron (**soc**)-topology have immense potential in practical applications owing to their promising properties, like preferable stability, chemical versatility and tailored functionality [28–30]. Iron being the 4th most abundant element in the earth crust and low toxicity further bolsters the development of iron containing MOFs. The **soc** topology MOFs (soc-MOFs) have microporous architectures with well-defined cages and channels and consist of narrow pores with higher localized charge density. These are built by a trigonal prismatic metal SBUs [$M_3(\mu_3\text{-}O)(-COO)_6$] connected via tetratopic organic linkers and exhibit distinct properties of high porosity, large gas storage capacity, and excellent thermal/chemical stability [28]. The introduction of functionalities on the ligand backbone can further augment the interactions with the gas molecules and lead to enhanced uptake capacities [31]. The soc-MOFs such as Al-soc-MOF-1 [32], In-soc-MOF-1a [33], BUT-22 [34] and other M(III)-soc-MOFs have already shown promising applications for gas (H_2, CH_4) storage and natural gas upgrading [28], whilst also showing high stability [35–38]. Here, we utilized a rigid tetracarboxylate linker featuring pyridine functionalities (H_4pbpta = 4,4′,4″,4‴-(1,4-phenylenbis(pyridine-4,2-6-triyl))-tetrabenzoic acid) and obtained Fe-pbpta with a very high Brunauer, Emmett and Teller (BET) surface area of 4,937 m^2/g. Fe-pbpta demonstrates highest gravimetric uptake of 369 cm^3(STP)/g under the DOE operational storage conditions (35 bar and 298 K), and also shows a high volumetric deliverable capacity of 192 cc/cc at 298 K and 65 bar.

2 Experimental section

2.1 Materials and methods

All reagents and solvents were purchased from commercial sources and used as received. The ligand H_4pbpta was synthesized from our previous reported procedure [39].

2.2 Synthesis of Fe-pbpta

A mixture of the ligand H_4pbpta (10 mg, 0.01 mmol) and $Fe(NO_3)_3{\cdot}9H_2O$ (18 mg, 0.045 mmol) was sonicated and dissolved in a 20 mL scintillation vial containing dimethylformamide (DMF) (1.2 mL) followed by the addition of acetic acid (0.25 mL). The vial was then placed in an oven at 135 °C for 24 h to yield yellow cubic crystals. Yield: 74.2% (based on the ligand). FTIR (cm^{-1}); ν = 3,061 (w, br.), 1,593 (m), 1,545 (m), 1,383 (s), 1,178 (w), 1,104 (w), 1,015 (m), 863 (w), 817 (m), 784 (s). Elemental analysis experimental: C, 56.47; H, 3.42; N, 3.56; calcd ($C_{66}H_{36}Fe_3N_3O_{16}$): C, 61.18; H, 2.78; N, 3.24.

2.3 Characterization

Powder X-ray diffraction (PXRD) data was collected at room temperature using a Bruker D8 Advance theta-2theta diffractometer with copper radiation (Cu Kα, λ = 1.5406 Å) and a secondary monochromator operating at 40 kV and 40 mA; whereby samples were measured between 3° and 30° at 0.6 s/step and step size of 0.02°. Single crystal X-ray diffraction (SCXRD) data were collected using synchrotron radiation (λ = 0.41328 Å) at the Advanced Photon Source Beamline 15-ID-B of ChemMatCARS in Argonne National Lab, Argonne, IL, USA. Infrared spectra measurements from 4,000–400 cm^{-1} were taken on a Perkin Elmer FT-IR Spectrometer Spectrum Two (UATR Two) with 4 cm^{-1} resolution. A TA Instruments TGA Q50 was used to record thermal gravimetric analysis (TGA) data from room temperature to 600 °C at a 10 °C/min rate. A Varian Unity Inova 400 spectrometer NMR was used to measure ^{1}H NMR. Low pressure gas adsorption measurements were performed using a Micromeritics ASAP 2020 analyzer for N_2 (surface area measurement at 77 K); and CH_4 isotherms at 273 and 298 K.

2.4 High pressure methane adsorption measurements

High-pressure adsorption isotherms in the range of 0–65 bar were measured on a HPVA-100 from Particulate Systems, a Micromeritics company. In a typical measurement, 0.26 g of activated sample was loaded into a tared 2 mL stainless steel sample holder inside a glove box under a N_2 atmosphere. Prior to connecting the sample holder to the vacuum coupling radiation (VCR) fittings of the complete high-pressure assembly inside the glove box, the sample holder was weighed to determine the sample mass. The sample holder was then transferred to the HPVA-100, connected to the analysis port via an VCR fitting, and evacuated at 140 °C for at least 10 h. A detailed description of the procedure used for measuring high-pressure CH_4 adsorption isotherms on the HPVA-100 was previously reported [40, 41]. We also tested methane adsorption on HKUST-1 as a reference and the excess uptake showed good agreement with the isotherm provided by Micromeritics (Fig. S11 in the Electronic Supplementary Material (ESM)).

2.5 Stability tests

In order to test the stability of the MOF under different environments, 40 mg of air-dried Fe-pbpta samples were soaked in 5 mL of water, and 5 mL aqueous solutions of 1 M HCl, 0.1 M NaOH and 1 M NaOH respectively for 24 h. Afterwards, the crystals were carefully decanted and washed with EtOH for several times. The resulting samples were then characterized using PXRD, BET and scanning electron microscopy (SEM). The samples were immersed in dichloromethane (DCM) overnight and activated at 140 °C for 10 h prior to the BET measurements.

3 Results and discussion

3.1 Structure description and characterizations

The Fe-pbpta was obtained as yellow cubic crystals from solvothermal reaction of high-valent $Fe(NO_3)_3$ and rigid tetracarboxylate ligand H_4pbpta in the presence of acetic acid as the modulator in DMF (Fig. 1). The SCXRD analysis revealed that Fe-pbpta crystallizes in the cubic $Pm\bar{3}n$ space group as $[Fe_3O(pbpta)_{1.5}(H_2O)_3]{\cdot}(NO_3)$. The crystal structure is similar to the other reported soc-MOFs [29, 32, 33, 35, 36, 38, 42–45]

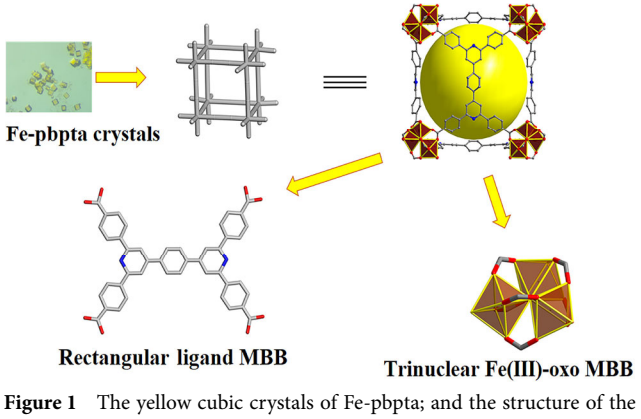

Figure 1 The yellow cubic crystals of Fe-pbpta; and the structure of the framework built from trinuclear iron(III) MBB [$Fe_3(\mu_3\text{-}O)(H_2O)_3(-COO)_6$] and rectangular tetracarboxylate ligand $pbpta^{4-}$.

whereby the inorganic molecular building blocks (MBBs) are composed of μ_3-oxo-centered trinuclear Fe(III) clusters; and the $[Fe_3(\mu_3\text{-}O)(H_2O)_3(\text{–}COO)_6]$ MBBs are bridged by six independent $pbpta^{4-}$ ligands to form a 3-periodic cationic Fe-pbpta framework. Each Fe^{3+} cation adopts an octahedral coordination environment composed of six oxygen atoms, of which four are from bis-monodentate deprotonated carboxylate oxygens from four independent $pbpta^{4-}$ ligands, one is the μ_3-oxo anion, and one is the terminal oxygen that completes the coordination sphere (Fig. 1). The charge balance in the framework can either be provided by the ^{-}OH anions on the cluster, or the presence of nitrate anions that could be disordered in the framework. Due to the poor resolution of diffraction data and high symmetry of the framework, the nitrate anions could not be located properly inside the pores of the framework. Elemental analysis and FTIR (Fig. S1 in the ESM) characterizations were further inconclusive in determination of the anion.

Considering the trinuclear Fe(III) cluster as trigonal prismatic SBU with the six carbons of the carboxylate moieties as 6-c node and the rectangular organic ligand as the 4-c node, the topological analysis reveals that the network has the edge transitive (4,6)-connected net with the underlying **soc** topology. The overall three-dimensional (3D) porous framework contains embedded cubic cages (volume 18.2 Å × 18.2 Å × 18.2 Å), window dimension of 11.0 Å × 9.0 Å that are interconnected through square channels along the three directions. The solvent accessible free volume for Fe-pbpta was estimated to be 75% using PLATON software.

The phase purity of the bulk sample was confirmed by comparing the experimental PXRD pattern to the calculated PXRD pattern obtained from the single crystal structure using Mercury software which were in excellent agreement with each other (Fig. S3 in the ESM). The thermal gravimetric analysis showed a good thermal stability up to 350 °C (Fig. S2 in the ESM) with first release of solvent at 60 °C.

In order to achieve proper activation of the MOF material, the guest molecules in the as-synthesized sample were exchanged with methanol followed by DCM. Owing to the high stability of the pure microporous architecture, the solvent in the pores could then be removed by conventional activation methods (drying under dynamic vacuum at 140 °C for 10 h) and nitrogen adsorption measurements were carried out at 77 K. The material showed a reversible Type I isotherm typical of the microporous materials (Fig. 2) and displayed very high Langmuir and BET specific surface areas of 6,712 and 4,937 m^2/g respectively as well as a large pore volume of 2.15 cm^3/g. This remarkably high surface area has not been observed in case of iron-based MOFs and is one of the highest among the family of soc-MOFs reported thus far [29, 32, 33, 35, 36, 37, 42–45]. The observed pore width from the pore size distribution of 18 Å is in good agreement with the calculated pore width of 18.2 Å.

3.2 Stability measurements

In accordance with the hard and soft acids and bases (HSAB) theory, the carboxylate-based ligands as hard Lewis bases show very strong interactions with the high valent Fe^{3+} ions acting as hard Lewis acids. Also, the longer and rigid ligands impart additional stability to the resulting frameworks due to higher activation energy of decomposition in the transition states [46].

To test stability of the framework under operational conditions, we exposed the MOF to air and soaked it in water for 24 h. The Fe-pbpta shows high stability of the framework in air and aqueous conditions. As can be seen from the PXRD patterns and SEM images in Figs. 3 and 4 respectively, the Fe-pbpta retains its crystallinity after being subjected to air and water for 24 h. The N_2 sorption isotherms remain almost the same as the pristine framework (Fig. S7 in the ESM), further establishing the stability of the MOF under these conditions.

To test its chemical stability, we exposed the sample to acidic (1 M aqueous HCl) and basic (pH 11–14) conditions. Under the acidic conditions, structural defects are probably introduced and the framework undergoes slight loss in crystallinity evident from the reduction in intensity of relative peaks and peak broadening in the PXRD pattern (Fig. S6 in the ESM). Furthermore, there is a slight loss in porosity of the framework indicated by the reduced N_2 uptake at 77 K (Fig. S7 in the ESM). Upon increasing the pH to 11, there is a similar loss of crystallinity. Further increasing the pH, the framework undergoes decomposition and completely loses its crystallinity (Fig. S6 in the ESM). Fe-pbpta is among the MOFs based on the $[Fe_3(\mu_3\text{-}O)(\text{–}COO)_6]$ clusters showing good air/water stability such as MIL-101(Fe) and MIL-53(Fe). Its chemical stability over the wider pH range from 1–11 is however less than PCN-333 (Fe), PCN-250 (Fe) and PCN-600 (Fe) which show very high stability under these conditions [46].

The high porosity and bulk phase purity of the material, ability to be activated under traditional activation conditions and high air/aqueous stability of the framework made it an ideal candidate for onboard or stationary methane storage studies.

3.3 Methane adsorption

The Fe-pbpta was first evaluated for its methane uptake capacities

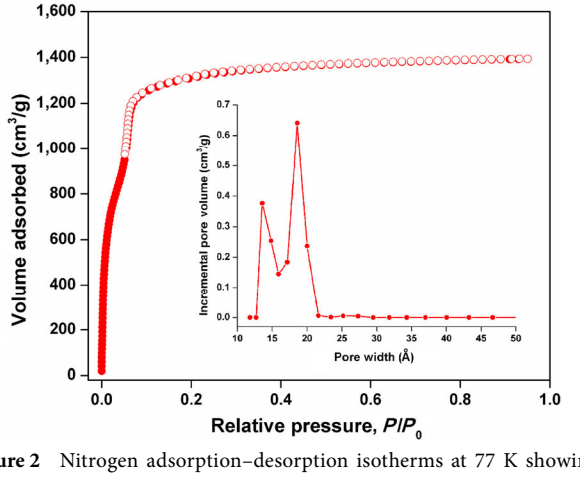

Figure 2 Nitrogen adsorption–desorption isotherms at 77 K showing very high uptake reaching 1,400 cm^3(STP)/g. The pore size distribution is provided in the inset.

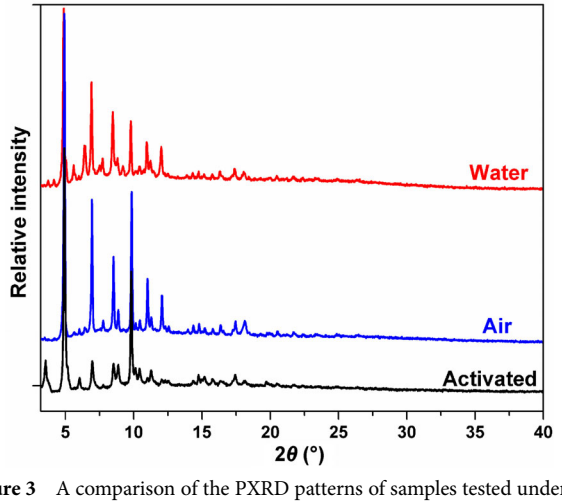

Figure 3 A comparison of the PXRD patterns of samples tested under air and aqueous environment.

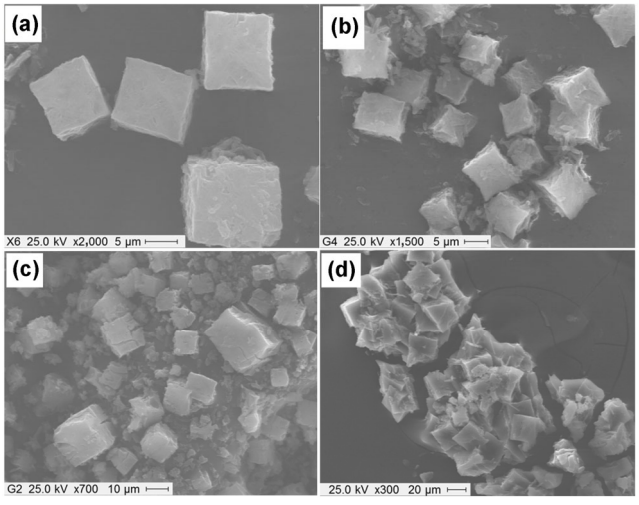

Figure 4 SEM images of samples as synthesized (a), air (b), water (c) and acid (d).

in the low-pressure region and quite interestingly, it showed very moderate methane uptake at 273 and 298 K with pressures reaching up to 1 bar (Fig. S8 in the ESM). Such behavior is desirable for MOFs in order to achieve high working capacities, i.e. low uptake at lower pressures and high uptake as the pressures increase. The isosteric heat of adsorption (Q_{st}) was also calculated at zero coverage using dual-site Langmuir-Freundlich (DSLF) model and turned out to be 22.27 kJ/mol (Fig. S9 in the ESM). Upon carrying out the high-pressure methane uptake measurements at 273 and 298 K, Fe-pbpta showed a total gravimetric uptake of 369 cm^3(STP)/g under the DOE operational storage conditions (35 bar and 298 K) (Fig. 5(a)). This uptake capacity is comparable to other microporous Al-soc-MOF-1 [32] (361 cm^3/g), mesoporous MOF-210 [47] (210 cm^3/g) and DUT-49 [48] (364 cm^3/g) under the same conditions. The gravimetric uptake capacity at 65 bar and 298 K reaches 579 cm^3/g, and the current gravimetric DOE target of 700 cm^3(STP)/g could be achieved at 52 bar and 273 K (Fig. 5(a)).

The deliverable capacity is more relevant compared to the total gravimetric uptake for operational usage of a material. The gravimetric uptake capacity of 0.37 g/g for Fe-pbpta at 65 bar and 298 K is among one of the highest reported for MOFs. It is higher than MOF-205 (0.32 g/g), MOF-177 (0.30 g/g) and BUT-22 (0.295); and comparable to Al-soc-MOF-1 (0.37) and DUT-49 (0.36 g/g). The selected MOF materials with their total gravimetric uptakes and deliverable capacities at 65 bar and 298 K are shown in Fig. 6.

The volumetric methane uptake capacities were calculated using the crystal density of Fe-pbpta (0.376 g/cm^3). The total volumetric uptake capacity of 219 cc/cc at 298 K and 65 bar (Fig. 5(b)) is comparable to Al-soc-MOF-1 [32], Fe(bdp) and Co(bdp) [25] having uptake capacities of 198, 196 and 205 cc/cc, respectively, under the same conditions.

The deliverable volumetric capacities (5–35 bar) increased from 116 to 167 cc/cc upon decreasing the temperature from 298 to 273 K, a phenomenon being observed only recently for MOFs such as Al-soc-MOF-1 [32] and Cu-tbo-MOF-5 [49] which show this increase opposite to that of other MOFs such as HKUST-1, Ni-MOF-74, NU-111 [16] and UTSA-76a [21].

In the 5–65 bar regime, the Fe-pbpta showed a high deliverable capacity of 192 cc/cc at 298 K which is more than Al-soc-MOF-1 [32] (176 cc/cc) and MAF-38 [22] (187 cc/cc); and comparable to HKUST-1 [16] (190 cc/cc), Fe(bdp) (190 cc/cc), Co-bdp [25] (197 cc/cc) and UTSA-76a [21] (197 cc/cc). A comparison of the selected high performing MOFs at 65 bar and 298 K is provided in Fig. 7.

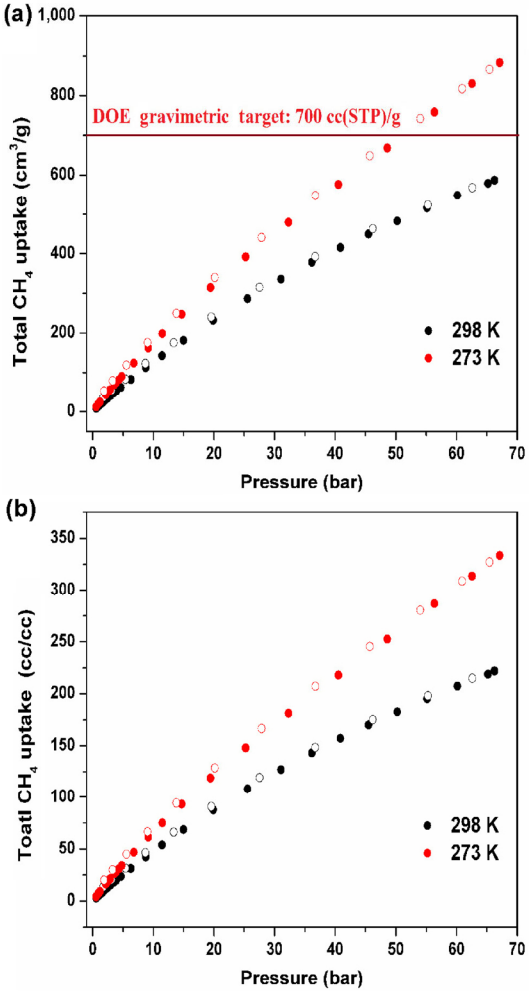

Figure 5 (a) The total gravimetric uptake at 273 K (red circles) and 298 K (black circles) and (b) the total volumetric uptake at 273 K (red circles) and 298 K (black circles).

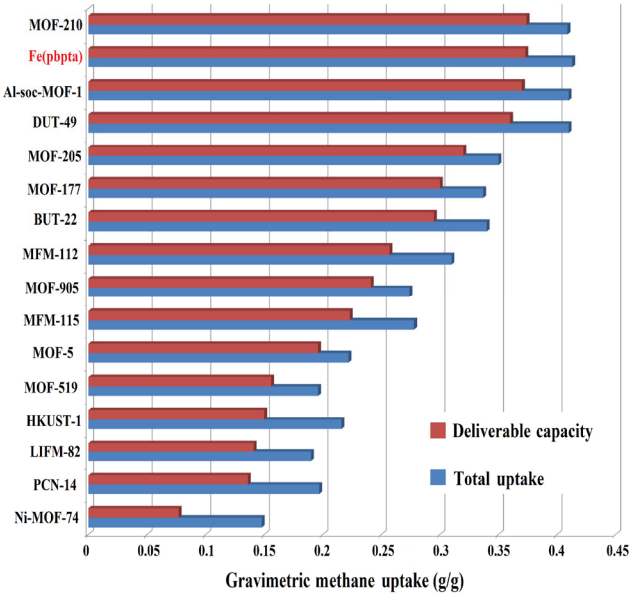

Figure 6 A comparison of the total gravimetric methane uptake (blue) and deliverable capacity (red) of top performing MOFs at 298 K and 65 bar.

The deliverable capacity reaches 288 cc/cc at 273 K making it a promising candidate for meeting the DOE targets of 350 cc/cc at higher pressures and lower temperatures. A comparison of Fe-pbpta with other MOFs is provided in Table S7 in the ESM.

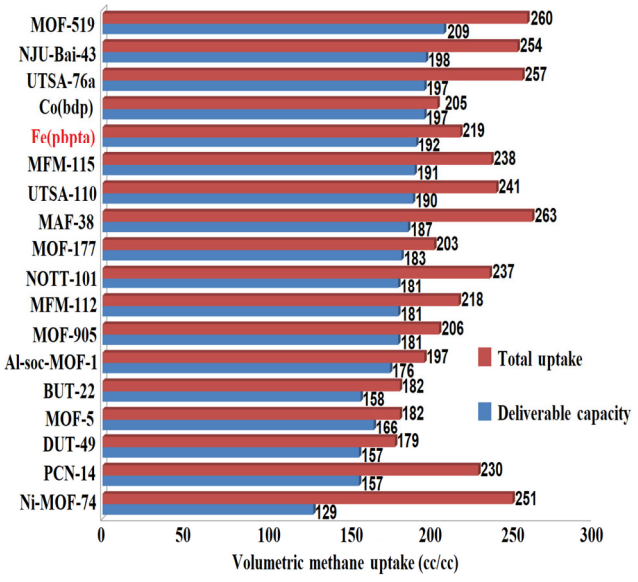

Figure 7 A comparison of total volumetric methane uptake (red) and deliverable capacity (blue) at 65 bar and 298 K for selected MOFs.

The appropriate pore size of Fe-pbpta leads to enhanced methane–methane interactions [32] at high pressures and the presence of Lewis basic pyridine nitrogen atoms further increases the methane uptake at high pressures reaching to 65 bar [31].

The high gravimetric and volumetric methane deliverable capacities, accompanied by its high aqueous and air stability make Fe-pbpta a good candidate for methane storage and delivery. Further insights into the methane binding sites and approaches to enhance the chemical stability would be investigated in the future.

4 Conclusion

In conclusion, we have successfully synthesized Fe-pbpta framework of **soc**-topology using a custom-designed ligand. The microporous architecture endows Fe-pbpta with high BET surface area of 4,937 m^2/g, one of the highest among the reported soc-MOFs and the highest among iron-based MOFs. In addition, Fe-pbpta exhibits good aqueous/air stability. Moreover, Fe-pbpta demonstrates great methane storage performance with an unprecedented total gravimetric methane uptake capacity of 369 cm^3(STP)/g under the DOE operational storage conditions (35 bar and 298 K) as well as a high total volumetric methane deliverable capacity of 192 cc/cc at 298 K and 65 bar. These results in totality promote ANG technology and make Fe-pbpta framework a promising candidate for on-board methane storage.

Acknowledgements

This material is based upon work supported by the U.S. Department of Energy's Office of Energy Efficiency and Renewable Energy under the Hydrogen and Fuel Cell Technologies and Vehicle Technologies Offices under Award Number DE-EE0008812. S. K. acknowledges the financial support from the University Grants Commission (UGC), New Delhi, India (No. F 5-80/2014(IC)). ChemMatCARS Sector 15 is principally supported by the Divisions of Chemistry (CHE) and Materials Research (DMR), National Science Foundation, under Grant Number NSF/CHE-1346572. Use of the Advanced Photon Source, an Office of Science User Facility operated for the U.S. Department of Energy (DOE) Office of Science by Argonne National Laboratory, was supported by the U.S. DOE under Contract No. DE-AC02-06CH11357. G. V. would further like to acknowledge Jason Exley (Sales Engineer, Micromeritics USA) for help and support provided with the measurements and the HKUST reference data.

Electronic Supplementary Material: Supplementary material (single crystal data, characterization data (PXRD, BET and Q_{st}) and supporting figures and tables) is available in the online version of this article at https://doi.org/10.1007/s12274-020-2794-9 .

References

[1] IEA (2017), *Energy Technology Perspectives 2017*, IEA, Paris. https://www.iea.org/reports/energy-technology-perspectives-2017 (accessed Dec 20, 2019).

[2] IPCC, 2018: *Global Warming of 1.5 °C. An IPCC Special Report on the impacts of global warming of 1.5 °C above pre-industrial levels and related global greenhouse gas emission pathways, in the context of strengthening the global response to the threat of climate change, sustainable development, and efforts to eradicate poverty*; Masson-Delmotte, V.; Zhai, P.; Pörtner, H. O.; Roberts, D.; Skea, J.; Shukla, P. R.; Pirani, A.; Moufouma-Okia, W.; Péan, C.; Pidcock, R. et al., Eds.; Intergovernmental Panel on Climate Change: 2018.

[3] Chu, S.; Cui, Y.; Liu, N. The path towards sustainable energy. *Nat. Mater.* **2017**, *16*, 16–22.

[4] He, Y. B.; Zhou, W.; Qian, G. D.; Chen, B. L. Methane storage in metal-organic frameworks. *Chem. Soc. Rev.* **2014**, *43*, 5657–5678.

[5] Li, B.; Wen, H. M.; Zhou, W.; Xu, J. Q.; Chen, B. L. Porous metal-organic frameworks: Promising materials for methane storage. *Chem* **2016**, *1*, 557–580.

[6] Kirchon, A.; Feng, L.; Drake, H. F.; Joseph, E. A.; Zhou, H. C. From fundamentals to applications: A toolbox for robust and multifunctional MOF materials. *Chem. Soc. Rev.* **2018**, *47*, 8611–8638.

[7] Song, Y. P.; Sun, Q.; Aguila, B.; Ma, S. Q. Opportunities of covalent organic frameworks for advanced applications. *Adv. Sci.* **2019**, *6*, 1801410.

[8] Lohse, M. S.; Bein, T. Covalent organic frameworks: Structures, synthesis, and applications. *Adv. Funct. Mater.* **2018**, *28*, 1705553.

[9] Burrows, A. D. The chemistry of metal-organic frameworks. Synthesis, characterization, and applications, 2 volumes. Edited by stefan kaskel. *Angew. Chem., Int. Ed.* **2017**, *56*, 1449.

[10] Yaghi, O. M.; O'Keeffe, M.; Ockwig, N. W.; Chae, H. K.; Eddaoudi, M.; Kim, J. Reticular synthesis and the design of new materials. *Nature* **2003**, *423*, 705–714.

[11] Kalmutzki, M. J.; Hanikel, N.; Yaghi, O. M. Secondary building units as the turning point in the development of the reticular chemistry of MOFs. *Sci. Adv.* **2018**, *4*, eaat9180.

[12] Eddaoudi, M.; Kim, J.; Rosi, N.; Vodak, D.; Wachter, J.; O'Keeffe, M.; Yaghi, O. M. Systematic design of pore size and functionality in isoreticular MOFs and their application in methane storage. *Science* **2002**, *295*, 469–472.

[13] Zhou, H. C.; Long, J. R.; Yaghi, O. M. Introduction to metal-organic frameworks. *Chem. Rev.* **2012**, *112*, 673–674.

[14] Lu, W. G.; Wei, Z. W.; Gu, Z. Y.; Liu, T. F.; Park, J.; Park, J.; Tian, J.; Zhang, M. W.; Zhang, Q.; Gentle, T., III. et al. Tuning the structure and function of metal-organic frameworks via linker design. *Chem. Soc. Rev.* **2014**, *43*, 5561–5593.

[15] Furukawa, H.; Cordova, K. E.; O'Keeffe, M.; Yaghi, O. M. The chemistry and applications of metal-organic frameworks. *Science* **2013**, *341*, 1230444.

[16] Peng, Y.; Krungleviciute, V.; Eryazici, I.; Hupp, J. T.; Farha, O. K.; Yildirim, T. Methane storage in metal-organic frameworks: Current records, surprise findings, and challenges. *J. Am. Chem. Soc.* **2013**, *135*, 11887–11894.

[17] Simon, C. M.; Kim, J.; Gomez-Gualdron, D. A.; Camp, J. S.; Chung, Y. G.; Martin, R. L.; Mercado, R.; Deem, M. W.; Gunter, D.; Haranczyk, M. et al. The materials genome in action: Identifying the performance limits for methane storage. *Energy Environ. Sci.* **2015**, *8*, 1190–1199.

[18] Li, H.; Wang, K. C.; Sun, Y. J.; Lollar, C. T.; Li, J. L.; Zhou, H. C. Recent advances in gas storage and separation using metal-organic frameworks. *Mater. Today* **2018**, *21*, 108–121.
[19] Chui, S. S. Y.; Lo, S. M. F.; Charmant, J. P. H.; Orpen, A. G.; Williams, I. D. A chemically functionalizable nanoporous material $[Cu_3(TMA)_2(H_2O)_3]_n$. *Science* **1999**, *283*, 1148–1150.
[20] Ma, S. Q.; Sun, D. F.; Simmons, J. M.; Collier, C. D.; Yuan, D. Q.; Zhou, H. C. Metal-organic framework from an anthracene derivative containing nanoscopic cages exhibiting high methane uptake. *J. Am. Chem. Soc.* **2008**, *130*, 1012–1016.
[21] Li, B.; Wen, H. M.; Wang, H. L.; Wu, H.; Tyagi, M.; Yildirim, T.; Zhou, W.; Chen, B. L. A porous metal-organic framework with dynamic pyrimidine groups exhibiting record high methane storage working capacity. *J. Am. Chem. Soc.* **2014**, *136*, 6207–6210.
[22] Lin, J. M.; He, C. T.; Liu, Y.; Liao, P. Q.; Zhou, D. D.; Zhang, J. P.; Chen, X. M. A metal-organic framework with a pore size/shape suitable for strong binding and close packing of methane. *Angew. Chem., Int. Ed.* **2016**, *55*, 4674–4678.
[23] Gándara, F.; Furukawa, H.; Lee, S.; Yaghi, O. M. High methane storage capacity in aluminum metal-organic frameworks. *J. Am. Chem. Soc.* **2014**, *136*, 5271–5274.
[24] Zhang, M. X.; Zhou, W.; Pham, T.; Forrest, K. A.; Liu, W. L.; He, Y. B.; Wu, H.; Yildirim, T.; Chen, B. L.; Space, B. et al. Fine tuning of MOF-505 analogues to reduce low-pressure methane uptake and enhance methane working capacity. *Angew. Chem., Int. Ed.* **2017**, *56*, 11426–11430.
[25] Mason, J. A.; Oktawiec, J.; Taylor, M. K.; Hudson, M. R.; Rodriguez, J.; Bachman, J. E.; Gonzalez, M. I.; Cervellino, A.; Guagliardi, A.; Brown, C. M. et al. Methane storage in flexible metal-organic frameworks with intrinsic thermal management. *Nature* **2015**, *527*, 357–361.
[26] Wen, H. M.; Li, B.; Li, L. B.; Lin, R. B.; Zhou, W.; Qian, G. D.; Chen, B. L. A metal-organic framework with optimized porosity and functional sites for high gravimetric and volumetric methane storage working capacities. *Adv. Mater.* **2018**, *30*, 1704792.
[27] Kundu, T.; Shah, B. B.; Bolinois, L.; Zhao, D. Functionalization-induced breathing control in metal-organic frameworks for methane storage with high deliverable capacity. *Chem. Mater.* **2019**, *31*, 2842–2847.
[28] Belmabkhout, Y.; Pillai, R. S.; Alezi, D.; Shekhah, O.; Bhatt, P. M.; Chen, Z. J.; Adil, K.; Vaesen, S.; De Weireld, G.; Pang, M. L. et al. Metal-organic frameworks to satisfy gas upgrading demands: Fine-tuning the soc-MOF platform for the operative removal of H_2S. *J. Mater. Chem. A* **2017**, *5*, 3293–3303.
[29] Pang, M. L.; Cairns, A. J.; Liu, Y. L.; Belmabkhout, Y.; Zeng, H. C.; Eddaoudi, M. Synthesis and integration of Fe-soc-MOF cubes into colloidosomes via a single-step emulsion-based approach. *J. Am. Chem. Soc.* **2013**, *135*, 10234–10237.
[30] Mavrandonakis, A.; Vogiatzis, K. D.; Boese, A. D.; Fink, K.; Heine, T.; Klopper, W. *Ab initio* study of the adsorption of small molecules on metal-organic frameworks with oxo-centered trimetallic building units: The role of the undercoordinated metal ion. *Inorg. Chem.* **2015**, *54*, 8251–8263.
[31] Li, B.; Wen, H. M.; Wang, H. L.; Wu, H.; Yildirim, T.; Zhou, W.; Chen, B. L. Porous metal-organic frameworks with Lewis basic nitrogen sites for high-capacity methane storage. *Energy Environ. Sci.* **2015**, *8*, 2504–2511.
[32] Alezi, D.; Belmabkhout, Y.; Suyetin, M.; Bhatt, P. M.; Weseliński, Ł. J.; Solovyeva, V.; Adil, K.; Spanopoulos, I.; Trikalitis, P. N.; Emwas, A. H. et al. MOF crystal chemistry paving the way to gas storage needs: Aluminum-based soc-MOF for CH_4, O_2, and CO_2 storage. *J. Am. Chem. Soc.* **2015**, *137*, 13308–13318.
[33] Cairns, A. J.; Eckert, J.; Wojtas, L.; Thommes, M.; Wallacher, D.; Georgiev, P. A.; Forster, P. M.; Belmabkhout, Y.; Ollivier, J.; Eddaoudi, M. Gaining insights on the H_2-sorbent interactions: Robust soc-MOF platform as a case study. *Chem. Mater.* **2016**, *28*, 7353–7361.
[34] Wang, B.; Zhang, X.; Huang, H. L.; Zhang, Z. J.; Yildirim, T.; Zhou, W.; Xiang, S. C.; Chen, B. L. A microporous aluminum-based metal-organic framework for high methane, hydrogen, and carbon dioxide storage. *Nano Res.*, in press, DOI: 10.1007/s12274-020-2713-0.
[35] Towsif Abtab, S. M.; Alezi, D.; Bhatt, P. M.; Shkurenko, A.; Belmabkhout, Y.; Aggarwal, H.; Weseliński, Ł. J.; Alsadun, N.; Samin, U.; Hedhili, M. N. et al. Reticular chemistry in action: A hydrolytically stable MOF capturing twice its weight in adsorbed water. *Chem* **2018**, *4*, 94–105.
[36] Zhang, J. W.; Qu, P.; Hu, M. C.; Li, S. N.; Jiang, Y. C.; Zhai, Q. G. Topology-guided design for Sc-soc-MOFs and their enhanced storage and separation for CO_2 and C_2-hydrocarbons. *Inorg. Chem.* **2019**, *58*, 16792–16799.
[37] Zhai, Q. G.; Bu, X. H.; Mao, C. Y.; Zhao, X.; Feng, P. Y. Systematic and dramatic tuning on gas sorption performance in heterometallic metal-organic frameworks. *J. Am. Chem. Soc.* **2016**, *138*, 2524–2527.
[38] Liu, Y. L.; Eubank, J. F.; Cairns, A. J.; Eckert, J.; Kravtsov, V. C.; Luebke, R.; Eddaoudi, M. Assembly of metal-organic frameworks (MOFs) based on indium-trimer building blocks: A porous MOF with **soc** topology and high hydrogen storage. *Angew. Chem., Int. Ed.* **2007**, *46*, 3278–3283.
[39] Verma, G.; Kumar, S.; Pham, T.; Niu, Z.; Wojtas, L.; Perman, J. A.; Chen, Y. S.; Ma, S. Q. Partially interpenetrated NbO topology metal-organic framework exhibiting selective gas adsorption. *Cryst. Growth Des.* **2017**, *17*, 2711–2717.
[40] Hulvey, Z.; Vlaisavljevich, B.; Mason, J. A.; Tsivion, E.; Dougherty, T. P.; Bloch, E. D.; Head-Gordon, M.; Smit, B.; Long, J. R.; Brown, C. M. Critical factors driving the high volumetric uptake of methane in $Cu_3(btc)_2$. *J. Am. Chem. Soc.* **2015**, *137*, 10816–10825.
[41] Mason, J. A.; Veenstra, M.; Long, J. R. Evaluating metal-organic frameworks for natural gas storage. *Chem. Sci.* **2014**, *5*, 32–51.
[42] Moellmer, J.; Celer, E. B.; Luebke, R.; Cairns, A. J.; Staudt, R.; Eddaoudi, M.; Thommes, M. Insights on adsorption characterization of metal-organic frameworks: A benchmark study on the novel soc-MOF. *Micropor. Mesopor. Mat.* **2010**, *129*, 345–353.
[43] Pang, M. L.; Cairns, A. J.; Liu, Y. L.; Belmabkhout, Y.; Zeng, H. C.; Eddaoudi, M. Highly monodisperse M^{III}-based soc-MOFs (M = In and Ga) with cubic and truncated cubic morphologies. *J. Am. Chem. Soc.* **2012**, *134*, 13176–13179.
[44] Bratsos, I.; Tampaxis, C.; Spanopoulos, I.; Demitri, N.; Charalambopoulou, G.; Vourloumis, D.; Steriotis, T. A.; Trikalitis, P. N. Heterometallic In(III)-Pd(II) porous metal-organic framework with square-octahedron topology displaying high CO_2 uptake and selectivity toward CH_4 and N_2. *Inorg. Chem.* **2018**, *57*, 7244–7251.
[45] Liu, H. Y.; Gao, G. M.; Bao, F. L.; Wei, Y. H.; Wang, H. Y. Enhanced water stability and selective carbon dioxide adsorption of a soc-MOF with amide-functionalized linkers. *Polyhedron* **2019**, *160*, 207–212.
[46] Yuan, S.; Feng, L.; Wang, K. C.; Pang, J. D.; Bosch, M.; Lollar, C.; Sun, Y. J.; Qin, J. S.; Yang, X. Y.; Zhang, P. et al. Stable metal-organic frameworks: Design, synthesis, and applications. *Adv. Mater.* **2018**, *30*, 1704303.
[47] Farha, O. K.; Özgür Yazaydın, A.; Eryazici, I.; Malliakas, C. D.; Hauser, B. G.; Kanatzidis, M. G.; Nguyen, S. T.; Snurr, R. Q.; Hupp, J. T. *De novo* synthesis of a metal-organic framework material featuring ultrahigh surface area and gas storage capacities. *Nat. Chem.* **2010**, *2*, 944–948.
[48] Stoeck, U.; Krause, S.; Bon, V.; Senkovska, I.; Kaskel, S. A highly porous metal-organic framework, constructed from a cuboctahedral super-molecular building block, with exceptionally high methane uptake. *Chem. Commun.* **2012**, *48*, 10841–10843.
[49] Spanopoulos, I.; Tsangarakis, C.; Klontzas, E.; Tylianakis, E.; Froudakis, G.; Adil, K.; Belmabkhout, Y.; Eddaoudi, M.; Trikalitis, P. N. Reticular synthesis of HKUST-like tbo-MOFs with enhanced CH_4 storage. *J. Am. Chem. Soc.* **2016**, *138*, 1568–1574.